Polyhedron 30 (2011) 2581–2591

Contents lists available at ScienceDirect

Polyhedron

journal homepage: www.elsevier.com/locate/poly

Redox-active metal(II) complexes of sterically hindered phenolic ligands: Antibacterial activity and reduction of cytochrome *c*. Part II. Metal(II) complexes of *o*-diphenol derivatives of thioglycolic acid

N.V. Loginova [a,*], T.V. Koval'chuk [a,b], Y.V. Faletrov [b], Y.S. Halauko [a], N.P. Osipovich [b], G.I. Polozov [a], R.A. Zheldakova [c], A.T. Gres [a], A.S. Halauko [a], I.I. Azarko [d], V.M. Shkumatov [a], O.I. Shadyro [a]

[a] *Faculty of Chemistry, Belarusian State University, Leningradskaya str. 14, 220030 Minsk, Belarus*
[b] *Research Institute for Physico-Chemical Problems of the Belarusian State University, Leningradskaya str. 14, 220030 Minsk, Belarus*
[c] *Faculty of Biology, Belarusian State University, Nezavisimosti Ave. 4, 220030 Minsk, Belarus*
[d] *Faculty of Physics, Belarusian State University, Bobruiskaya str. 5, 220030 Minsk, Belarus*

ARTICLE INFO

Article history:
Received 24 March 2011
Accepted 6 July 2011
Available online 27 July 2011

Keywords:
Metal(II) complexes
Sterically hindered phenolic ligands
DFT calculations
Cytochrome *c*
Cytochrome P450-reductase
Antibacterial activity

ABSTRACT

The synthesis and physico-chemical characterization of Fe(II) and Mn(II) complexes of 2-[4,6-di(*tert*-butyl)-2,3-dihydroxyphenylsulfanyl]acetic acid (HL^I) and 2-[4,6-di(*tert*-butyl)-2,3-dihydroxyphenylsulfinyl]acetic acid (HL^{II}) were carried out. The investigation of the molecular and electronic structure of Cu(II), Ni(II), Zn(II), Fe(II) and Mn(II) complexes has been performed within the density functional theory (DFT) framework. The computed properties were compared to the experimental ones, and molecular structures of the compounds were proposed based on the array of spectral data and quantum chemical calculations. Antibacterial activity of the Fe(II) and Mn(II) complexes was evaluated in comparison with Cu(II), Co(II), Ni(II) and Zn(II) complexes and three standard antibiotics; it was found to follow the order: (1) $Cu(L^I)_2 > Mn(L^I)_2 > HL^I > Ni(L^I)_2 > Zn(L^I)_2 > Fe(L^I)_2 > Co(H_2O)_2L^I$; (2) $Cu(L^{II})_2 > Co(L^{II})_2 > Ni(L^{II})_2 > Mn(H_2O)_2(L^{II})_2 > Fe(L^{II})_2 > HL^{II} > Zn(L^{II})_2$; their reducing ability (determined electrochemically) followed the same order. Spectrophotometric investigation was carried out in order to estimate the rate of the reduction of bovine heart cytochrome *c* with the ligands and their metal(II) complexes. The complexes $Cu(L^I)_2$, $Mn(L^I)_2$ and $Co(L^{II})_2$ with the high reducing ability were found to be characterized by the highest rates of Cyt *c* reduction. NADPH:cytochrome P450-reductase had no substantial effect on the rate of cytochrome *c* reduction with HL^I and HL^{II} ligands.

1. Introduction

Previously we have found that some mono- and di-substituted derivatives of sterically hindered phenolic ligands as well as their complexes with Cu(II), Co(II), Ni(II) and Zn(II) ions exhibit antimicrobial and antiviral activities, the complexes mostly demonstrating a higher level of activity than the parent ligands [1–6]. Furthermore, using the method of cyclic voltammetry, we have shown these compounds to be also of a pronounced reducing ability correlating with antimicrobial activity in a limited series of these compounds [5–7]. As the values of redox potentials govern the ability of compounds to participate in redox interactions, studying electrochemical properties of pharmacologically active compounds may provide a useful approach to evaluation of their ability to undergo redox transformations in biosystems and, particularly, mechanisms of antimicrobial activity. One of the possible types of biological macromolecular targets of redox-active antimicrobial agents may be comprised by cytochromes *c* which are components of mammalian and bacterial electron transport chains [8–15].

All these considerations prompted us to extend our research to other phenolic ligands and their metal(II) complexes. In the present work the reduction of bovine heart cytochrome *c* (Cyt *c*), selected as a plausible model of bacterial cytochrome *c*, with two derivatives of sterically hindered sulfur-containing phenolic ligands, 2-[4,6-di(*tert*-butyl)-2,3-dihydroxyphenylsulfanyl]acetic acid (HL^I) and 2-[4,6-di(*tert*-butyl)-2,3-dihydroxyphenylsulfinyl]acetic acid (HL^{II}) (see below),

* Corresponding author. Tel.: +375 172 09 55 16; fax: +375 172 26 46 96/26 55 67.
E-mail addresses: loginonv@yahoo.com, loginonv@gmail.com (N.V. Loginova).

0277-5387/$ - see front matter © 2011 Elsevier Ltd. All rights reserved.
doi:10.1016/j.poly.2011.07.008

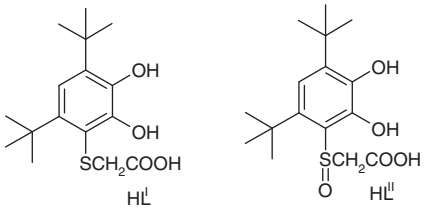

as well as with their redox-active transition metal (copper, cobalt, nickel, zinc, manganese, and iron) complexes was investigated spectrophotometrically. For the first time redox properties of above-mentioned ligands and their metal complexes were determined electrochemically. We also report here the synthesis and characterization of Fe(II) and Mn(II) complexes with aforesaid ligands in order to compare their coordinative behavior in relation to Fe(II), Mn(II) ions with the results obtained earlier for their Cu(II), Co(II), Ni(II) and Zn(II) complexes [16] and to assess the influence of complexation on their biological activity and redox properties.

Accurate molecular geometries are prerequisite for a reliable quantum chemical computation of properties. For molecules of moderate size composed of light atoms geometrical parameters can usually be calculated reliably at high *ab initio* levels. But for complexes, especially sterically hindered ones, the molecular geometries *a priori* can hardly be predicted for certain. The present work was focused up on the elucidation of molecular structures of mentioned complexes based on combination of spectral data and quantum chemical calculations. To give the assignment of vibrational spectra and to estimate molecular structures we applied quantum chemical calculations at the DFT level of theory using the B3PW91 hybrid functional with 6-31G(d) and LANL2DZ basis sets (including similar effective core potential) respectively for non-metals and metals. It has been proved earlier [17–21] that such an approach is sufficiently effective.

The results obtained are discussed in the context of presumed interconnection of the capacity of the compounds under study for reducing Cyt *c*, their antibacterial activity, redox properties determined electrochemically and other physico-chemical characteristics.

2. Experimental

2.1. Materials and methods

Chemicals were purchased from commercial sources and were used without further purification. 2-[4,6-Di(*tert*-butyl)-2,3-dihydroxyphenylsulfanyl]acetic acid (HL^I) and 2-[4,6-di(*tert*-butyl)-2,3-dihydroxyphenylsulfinyl]acetic acid (HL^{II}) were prepared according to the methods reported previously [16]. Synthesis of a structural analog of *o*-diphenol derivatives of thioglycolic acid (4,6-di(*tert*-butyl)-3-ethylsulfanyl-1,2-dihydroxybenzene) for the biological assay was performed as described in Section 2.8. The purity of compounds was checked by Thin Layer Chromatography (TLC). Elemental analyses were carried out with an instrument Vario EL (CHNS mode). Metals and sulfur were determined using an atomic emission spectrometer with an inductively coupled plasma excitation source (Spectroflame Modula). Infrared spectra of solids were recorded with a Nicolet 380 spectrometer in the wavelength range 4000–400 cm^{-1} at room temperature, using "Smart Performer"; spectra in the range 400–50 cm^{-1} were registered using "Vertex 70" instrument (Bruker Optik GmbH). Thermal analysis was performed with a Simultaneous Thermal Analyzer STA 449 C. X-ray diffraction (XRD) analysis was carried out with an HZG 4A diffractometer (Co Kα or Cu Kα radiation, MnO_2-filter). ESR (Electron Spin Resonance) spectra of polycrystalline samples were measured with ERS-220 *X*-band spectrometer (9.45 GHz) at room temperature and at 77 K, using 100-kHz field modulation; *g* factors were quoted relative to the standard marker 2,2-diphenyl-1-picrylhydrazyl (DPPH). The magnetic moment measurements of the investigated complexes were carried out using SQUID magnetometer. Ultraviolet–Visible (UV–Vis) absorption spectra were recorded with a SPECORD M500 spectrophotometer. The molar conductance of 10^{-3} mol l^{-1} solutions of the metal(II) complexes in acetonitrile was measured at 20 °C using a TESLA BMS91 conductometer (cell constant 1.0). The lipophilicity test was made by determining the *n*-octanol/water partition coefficient (P_{ow}) [22]. Electrochemical measurements were performed under dry nitrogen in a three-electrode two-compartment electrochemical cell using a glassy-carbon (GC) working electrode, Pt auxiliary electrode and Ag|AgCl|0.1 mol l^{-1} $(C_2H_5)_4NCl$ reference electrode. The supporting electrolyte was 0.1 mol l^{-1} $(C_2H_5)_4NClO_4$. The Ag|AgCl|0.1 mol l^{-1} $(C_2H_5)_4NCl$ reference electrode was calibrated with the ferrocenium|ferrocene redox couple located at $E_{1/2}$ = +0.54 V. Acetonitrile was used as a solvent.

2.2. Synthesis of the metal(II) complexes with 2-[4,6-di(tert-butyl)-2,3-dihydroxyphenylsulfanyl]acetic acid (HL^I) and 2-[4,6-di(tert-butyl)-2,3-dihydroxyphenylsulfinyl]acetic acid (HL^{II})

Based on our previous findings [1,2,16], the preparation of metal(II) complexes followed a common procedure. A solution of 0.05 mmol $M(CH_3COO)_2$ (M = Fe(II) and Mn(II)) in 10 ml of water was added dropwise to a colorless solution of 0.100 mmol of a ligand dissolved in 10 ml of ethanol (molar ratio M(II):L = 1:2). As these ligands can be oxidized by oxygen, argon was bubbled through the solutions (pH ≤6) during the synthesis to ensure the absence of oxygen. Precipitates of Fe(II) and Mn(II) complexes formed instantaneously. After 1.5 h stirring, they were collected on 0.2 μm membrane filters, washed with ethanol and water and dried *in vacuo* (yield >70%).

2.2.1. $Cu(L^I)_2$, $Co(H_2O)_2L^I$, $Ni(L^I)_2$ and $Zn(L^I)_2$ complexes

For elemental analyses data of these metal complexes see Ref. [16].

2.2.2. $Fe(L^I)_2$ complex

Blue. Yield: 73–75%. *Anal.* Calc. for $C_{32}H_{46}S_2O_8Fe$: C, 56.61; H, 6.84; S, 9.45; Fe, 8.23. Found: C, 56.54; H, 6.82; S, 9.38; Fe, 8.16%.

2.2.3. $Mn(L^I)_2$ complex

White. Yield: 75–80%. *Anal.* Calc. for $C_{32}H_{46}S_2O_8Mn$: C, 56.69; H, 6.84; S, 9.47; Mn, 8.11. Found: C, 56.62; H, 6.78; S, 9.41; Mn, 8.05%.

2.2.4. $Cu(L^{II})_2$, $Co(L^{II})_2$, $Ni(L^{II})_2$ and $Zn(L^{II})_2$ complexes

For elemental analyses data of these metal complexes see Ref. [16].

2.2.5. $Fe(L^{II})_2$ complex

Blue. Yield: 70–72%. *Anal.* Calc. for $C_{32}H_{46}S_2O_{10}Fe$: C, 54.06; H, 6.53; S, 9.03; Fe, 7.86. Found: C, 55.98; H, 6.43; S, 8.92; Fe, 7.77%.

2.2.6. $Mn(H_2O)_2(L^{II})_2$ complex

White. Yield: 75–80%. *Anal.* Calc. for $C_{32}H_{50}S_2O_{12}Mn$: C, 51.54; H, 6.71; S, 8.59; Mn, 7.38. Found: C, 51.49; H, 6.77; S, 8.54; Mn, 7.32%.

2.3. Physico-chemical characterization

2.3.1. $Cu(L^I)_2$, $Co(H_2O)_2L^I$, $Ni(L^I)_2$ and $Zn(L^I)_2$ complexes

For physical and spectral characteristics of these metal complexes see Refs. [1,16].

2.3.2. $Fe(L^I)_2$ complex

Molar conductivity (in acetonitrile): Λ_{mol}=6.9 Ω^{-1} cm^2 mol^{-1}. Thermogravimetric/differential thermal analysis (TG/DTA) data: no weight loss was observed until decomposition which began about 170 °C, with an exothermic peak at 200 °C and an endothermic one at 335 °C, ultimately leaving FeO as the residue. The maximal weight loss of 88.6% corresponds to the loss of two ligand molecules in the $Fe(L)_2$ complex (Calc. 89.4%). Prominent IR absorption bands (ν, cm^{-1}): 3429m (O–H), 1383m (COO$^-$), 1473m (C=C arom), 1188m, 1113m and 1025m (C–O), 757w and 668m (C–S), 582m and 532m (Fe–O), 345w (Fe–S). UV–Vis data (acetonitrile) (λ_{max}, nm (log ε)): 665 (2.34), 600 (2.29), 420 (3.32), 310 (3.72), 300 (3.65), 240 (3.94), 225 (3.99). μ_{eff} (RT, BM) = 0.

2.3.3. $Mn(L^I)_2$ complex

Molar conductivity (in acetonitrile): Λ_{mol} = 10.3 Ω^{-1} cm^2 mol^{-1}. TG/DTA data: no weight loss was observed until decomposition which began about 210 °C, with an endothermic peak at 285 °C, ultimately leaving MnO as the residue. The maximal weight loss of 88.3% corresponds to the loss of two ligand molecules in the $Mn(L^I)_2$ complex (Calc. 89.5%). Prominent IR absorption bands (ν, cm^{-1}): 3446w (O–H), 1395 m (COO$^-$), 1474w (C=C arom.), 1189m, 1175m, 1115m and 1026m (C–O), 668m (C–S), 582w, 531m and 509w (Mn–O), 335w (Mn–S). UV–Vis data (acetonitrile) (λ_{max}, nm (log ε)): 660 (2.39), 595 (2.55), 490 (3.56), 410 (3.65), 315 (3.74), 295 (3.79), 245(3.96). ESR data: g_{iso} = 2.015 (ΔH = 270 G). μ_{eff} (RT, BM) = 1.75.

2.3.4. $Cu(L^{II})_2$, $Co(L^{II})_2$, $Ni(L^{II})_2$ and $Zn(L^{II})_2$ complexes

For physical and spectral characteristics of these metal complexes see Ref. [16].

2.3.5. $Fe(L^{II})_2$ complex

Molar conductivity (in acetonitrile): Λ_{mol} = 4.9 Ω^{-1} cm^2 mol^{-1}. TG/DTA data: no weight loss was observed until decomposition which began about 165 °C, with a broad exothermic peak at 230 °C, leaving FeO as the residue. The maximal weight loss of 88.9% corresponds to the loss of two ligand molecules in the $Fe(L)_2$ complex (Calc. 89.9%). Prominent IR absorption bands (ν, cm^{-1}): 3625s, 3391s and 3286m (O–H), 1577m and 1390m (COO$^-$), 1485m (C=C arom.), 1168m and 1131m (C–O), 1023m (S=O), 686w and 612m (C–S), 562m, 584m and 472m (Fe–O). UV–Vis data (acetonitrile) (λ_{max}, nm (log ε)): 650 (2.31), 560 (2.51), 338 (3.58), 305 (3.67), 255 (3.71), 225 (3.85). μ_{eff} (RT, BM) = 0.

2.3.6. $Mn(H_2O)_2(L^{II})_2$ complex

Molar conductivity (in acetonitrile): Λ_{mol} = 11.0 Ω^{-1} cm^2 mol^{-1}. TG/DTA data: no weight loss was observed until decomposition which began about 65 °C, with an endothermic peak at 107 °C which corresponds to the loss of two water molecules (found: 4.27%, Calc. 4.83%) and with a broad exothermic peak in the temperature range 180–300 °C, ultimately leaving MnO as the residue. The maximal weight loss of 89.5% corresponds to the loss of two ligand molecules in the $Mn(H_2O)_2(L^{II})_2$ complex (Calc. 90.5%). Prominent IR absorption bands (ν, cm^{-1}): 3625s, 3419w (O–H), 1575m (COO$^-$), 1494m (C=C arom.), 1171m, 1135m, 1085m and 1046m (C–O), 1027m (S=O), 696m and 617m (C–S), 582w, 531m and 509w (Mn–O). UV–Vis data (acetonitrile) (λ_{max}, nm (log ε)): 645 (2.39), 590 (2.55), 343 (3.56), 315 (3.74), 297 (3.79), 258 (3.88), 228 (3.96). ESR data: g_{iso} = 2.02 (ΔH = 390 G). μ_{eff} (RT, BM) = 1.72.

2.4. Computational details

All calculations were performed using the GAUSSIAN03 software package [23]. MO calculations were carried out using the density functional theory B3PW91 method. Optimized geometries and single point energies of complexes were determined using the combined 6-31G(d) + LANL2DZ [24] basis set (for non-metal and metal atoms, respectively). In order to perform stationary points characterization and to calculate zero-point vibrational energies (ZPVE) and thermal corrections to Gibbs free energy, harmonic vibrational frequencies were calculated for structures obtained at the same level of theory. No special symmetry constraints were implemented during the optimization process. Regarding the conformational flexibility of the complexes, their initial structures were relaxed in TINKER program [25] prior to the DFT geometry optimization. At the particular level of theory a scaling factor of 0.951 [26] was applied to the frequencies in order to obtain better agreement with the experimental data.

To better understand the electronic structure of the complexes, the Mulliken orbital population analysis was performed. The redox properties were connected with the energies of the frontier orbitals by using Koopmans theorem: ionization energy = $-E$(HOMO) and electron affinity = E(LUMO).

2.5. Antibacterial assays

The following test microorganisms (collection of Department of Microbiology, Belarusian State University) were used: *Escherichia coli, Pseudomonasaeruginosa, Serratiamarcescens, Salmonella typhimurium, Bacillus subtilis, Sarcina lutea, Staphylococcus saprophyticus, Staphylococcus aureus, and Mycobacterium smegmatis.*

The antibacterial activity of the compounds was tested *in vitro* using the twofold serial dilutions (from 200 to 3.1 μg ml^{-1}) in liquid broth method for determination of a minimum inhibitory concentration (MIC, μg ml^{-1}) as described elsewhere [27]. The microorganisms stored in Muller–Hinton broth (Merck), were subcultured for testing in the same medium and grown at 37 °C. Then the cells were suspended, according to the McFarland protocol, in saline solution, to produce a suspension of about 10^5 CFU/ml (colony-forming units per ml). Serial dilutions of the test compounds, previously dissolved in dimethyl sulfoxide (DMSO), were carried out in test tubes to certain concentrations. Hundred milliliter of a 24 h old inoculum was added to each tube. The MIC, defined as the lowest concentration of the test compound, which inhibits the visible microbial growth, was determined after an incubation period of 24 h at 37 °C for bacteria. Tests using DMSO as a negative control were carried out in parallel. The amount of DMSO in the medium was 1% and did not affect the growth of the tested microorganisms. Commonly used antibiotics (streptomycin, tetracycline and chloramphenicol) were tested as positive controls. There were three replicates for each dilution. Results were always verified in three separate experiments.

2.6. Reduction of cytochrome c

Bovine heart cytochrome *c* (Sigma) was used. Human P450R was purified according to [28,29]. Spectrophotometric experiments were performed with a Shimadzu UV-1202 spectrophotometer using quartz cuvette with 1 cm optical path. Cyt *c* concentration was determined on its interaction with excess sodium dithionite, using the absorption coefficient ε_{550} = 21 mmol^{-1} l cm^{-1} [30]. Ar-saturated acetonitrile solutions of the ligands and complexes under

study and Cyt *c* (7 μmol l^{-1}) were used. Experiments were performed in 10 mmol l^{-1} sodium phosphate buffer (pH 7.4) at 20 °C. Aliquots of the compounds under study were added to Cyt *c* solution up to the final concentrations 35.0 or 17.4 μmol l^{-1}; if necessary, P450R was first added to Cyt *c*. The initial rate of Cyt *c* reduction (v) was evaluated by the slope of the kinetic curve A_{550} versus time according to [31,32]. The results were confirmed in three independent experiments.

2.7. Docking of the sterically hindered phenolic ligands with P450R

To evaluate a possible contribution of electrostatic repulsion into interaction of P450R with sterically hindered phenolic ligands under study, docking experiments of the above-mentioned ligand structures in the active center of P450R were carried out. Automated docking simulations were conducted with Autodock 4.0 software; the Graphical User Interface program "AutoDockTools" (The Scripps Research Institute) was used to prepare, run and analyze the docking simulations [33,34]. P450R 3D-structure was from RCSB protein database (PDB ID: 1b1c). Gasteiger partial charges were calculated and assigned to the atoms of flavin mononucleotide (FMN) and amino acid residues of the P450R [35]. The structures of the ligands were prepared using HyperChem (Hypercube). The simulation space was defined as a $60 \times 60 \times 60$ Å^3 box, which included FMN and closely disposed amino acid residues. The ligands were docked by the Lamarckian genetic algorithm default protocol. For each conformation interaction constant (K_{int}) values were calculated from docking energy (the sum of the intermolecular interaction energy and the ligand's internal energy) by AutoDock. Additionally, the least distances between phenolic oxygen atoms of the ligands and N5 atom of FMN (L_{min}(O–N))were calculated using AutoDockTools; both L_{min}(O–N) value for each ligand under study and the corresponding K_{int} value were tabulated.

2.8. Synthesis of 4,6-di(tert-butyl)-3-ethylsulfanyl-1,2-dihydroxybenzene (HL^V) – a structural analog of o-diphenol derivatives of thioglycolic acid for the biological assay

Ten millimolar of 3,5-di-*tert*-butyl-1,2-benzoquinone were added to the solution of 13.5 mmol ethanethiol in 40 ml hexane under stirring and cooling by ice water. An hour later the light-green solution was boiled dry under vacuum, the residue was dissolved in petroleum ether; the solution was filtered through a silica gel layer. The filtrate was boiled dry under vacuum, and the residue was recrystallized from hexane with the resulting separation of white crystals (yield >55%). M.p.: 93 °C. *Anal.* Calc. for $C_{16}H_{26}O_2S$: C, 68.04; H, 9.28; S, 11.35. Found: C, 55.98; H, 6.43; S, 8.92%. Mass spectrum (m/z, I%): 281.05 (M^+, 37), 267.05 ($M-CH_3$, 100). ^{1}H NMR δ_H (100 MHz, $CDCl_3$): 6.93 [s, 1H, aromatic H], 5.59 [s, 1H, OH], 2.66 [dd, 2H, CH_2], 1.51 [s, 9H, Me_3C], 1.42 [s, 9H, Me_3C], 1.31 [t, 3H, Me].

3. Results and discussion

3.1. Physico-chemical characterization

The solid products resulting from the interaction of Fe(II) and Mn(II) ions with HL^I and HL^{II} ligands were well characterized by means of elemental analysis, TG/DTA, FT-IR, UV–Vis, ESR, magnetic susceptibility and conductance measurements. The elemental analysis data for the Mn(II) and Fe(II) complexes with the ligand HL^I and the Fe(II) complex with the ligand HL^{II} are in agreement with the general formula ML_2 (Sections 2.2.2, 2.2.3 and 2.2.5), and for Mn(II) complex with the ligand HL^{II} – $Mn(H_2O)_2(L^{II})_2$ (Section 2.3.6). The data of thermal analysis performed in nitrogen atmosphere with identification of the final products by X-ray powder diffraction have shown the agreement between the experimental and theoretical weight losses for the processes of thermal decomposition of metal complexes (Sections 2.3.2, 2.3.3 and 2.3.5–2.3.6). These results confirm the above-mentioned two general formulas of the metal complexes.

The complexes were insoluble in water, ethanol, methanol, diethyl ether, but they were soluble in acetonitrile and dimethyl sulfoxide. The conductivity data indicate their being essentially non-electrolytes in acetonitrile [36] and suggest that the two bidentate ligands may be coordinated to Fe(II) and Mn(II) ions as monoanionic species.

No single crystals of Fe(II) and Mn(II) complexes suitable for X-ray diffraction studies were obtained because of the well-known difficulties of precipitating metal complexes with redox-active sterically hindered ligands from solutions [37]. The geometrical arrangement of the ligating atoms in the metal complexes was investigated by several spectroscopic and magnetochemical methods. The experimental studies on the synthesized metal complexes have been accompanied computationally by DFT which is commonly used to examine the electronic structure and geometrical parameters of transition metal complexes [38,39].

Most of the complexes under study can potentially exist as various geometrical isomers, where a metal ion is chelated by the ligand in different ways as shown in Fig. 1.

In order to identify the molecular structures and especially the coordination polyhedron of the complexes discussed in this work, we have analyzed their experimental vibrational spectra and com-

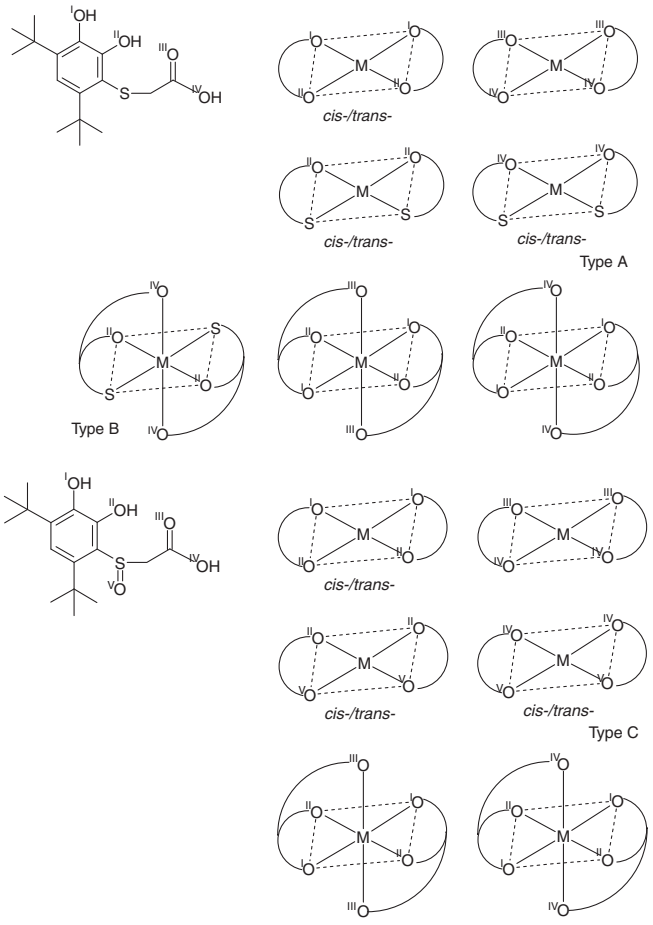

Fig. 1. Plausible coordination cores for metal complexes of ML_2 composition.

pared them with the calculated ones. It should be noted that this approach allows one to predict the general coordination pattern only, but it is very useful in our case for the lack of crystallographic data. From the following discussion one can see that the coordination type can be confidently specified relying on IR spectra. As for quantum chemical calculations, they allow one to distinguish between *cis* and *trans* configuration of the metal complex.

To specify the coordination cores in the Fe(II) and Mn(II) complexes, we used IR spectroscopy (Sections 2.3.2, 2.3.3 and 2.3.5–2.3.6). In the spectrum of the ligand HL^I there are three broad bands in the range from 3545 to 3349 cm^{-1}, which are evidence of intermolecular hydrogen bonds involving phenolic hydroxyl groups [40]. IR spectral assignments of the ligand HL^I, $Fe(L^I)_2$ and $Mn(L^I)_2$ complexes are indicative of metal(II) being coordinated with hydroxyl of the ligand HL^I: only one sharp band (3446 or 3429 cm^{-1}) is present in the spectra of metal complexes; the absorption bands corresponding to the stretching C–O bond vibrations are shifted to the lower frequency region, suggesting that the ligand is coordinated in the form of monoanion [40]. The shift of the bands at 775 and 677 cm^{-1} (assigned to C–S bond vibrations) in the spectra of $Fe(L^I)_2$, $Mn(L^I)_2$ complexes toward the low-frequency region suggests that sulfur is involved in the complexation. Instead of the characteristic bands of COOH group stretching vibrations at 1760–1740 cm^{-1} new bands appear in the spectra of these metal complexes at 1600–1573 cm^{-1}, characteristic of COO^--anion coordinated to a metal ion. It should be noted that in the spectra of $Fe(L^I)_2$ and $Mn(L^I)_2$ complexes there are new bands in the region from 580 to 470 cm^{-1}, which may be assigned to the stretching vibrations of M–O bonds [40]. M–S stretching vibration frequencies are registered in the region 350–330 cm^{-1}.

In the IR spectrum of the ligand HL^{II} there are three broad bands at 3510, 3463, 3348 cm^{-1}, which undergo changes in the spectra of its metal complexes (Sections 2.3.5 and 2.3.6), which may be due to a free and a hydrogen-bond bound hydroxyl groups in metal complex molecules [41]. A broad band in the range 3391–3200 cm^{-1} and a band at 899 cm^{-1} assigned to M–OH_2 vibrations present in the spectrum of $Mn(H_2O)_2(L^{II})_2$ complex substantiate the participation of water molecules in forming the coordination core of the complex and agree with the elemental analysis data for this complex. In the spectra of metal complexes for the ligand HL^{II} neither the bands resulting from the stretching vibrations of C–S bond change their position or intensity, nor the vibration bands in the range 380–300 cm^{-1} characteristic of M–S bond appear, thus suggesting that there is no coordination binding of sulfur atom to metal ion. Besides, a band at 1580–1575 cm^{-1} characteristic of stretching vibrations of COO^- group appears in their spectra instead of the band at 1715 cm^{-1} (that of stretching vibrations of COOH group) present in the spectrum of the parent HL^{II} ligand. In the spectra of $Fe(L^{II})_2$ and $Mn(H_2O)_2(L^{II})_2$ complexes a shift of the characteristic band of S=O group is observed, which is due to coordination binding of oxygen atom of this group. The strong bands in the range 590–415 cm^{-1} in the spectra of these complexes belong to M–O bonds [40].

The changes in the frequencies of (C=C) stretching vibrations of aromatic ring in the spectra of all metal complexes compared to those of the ligand HL^I (1487 cm^{-1}) or the ligand HL^{II} (1602 cm^{-1}) also are evidence in favor of the coordination bond formation.

The above-listed facts suggest that sulfanyl, sulfinyl and carboxylate groups as well as deprotonated hydroxyls take part in forming the MS_2O_4 or MO_4 coordination cores in the metal(II) complexes under study.

The ESR spectra of $Mn(L^I)_2$ and $Mn(H_2O)_2(L^{II})_2$ complexes show a broad isotropic signal (270 and 390 G, respectively) at liquid nitrogen temperature with g_{iso} values of 2.015 and 2.020, respectively. According to [42,43], such parameters are characteristic of Mn(II) complexes with a distorted octahedral coordination core and with virtually no interaction between manganese atoms. No signal of stabilized semiquinone radicals is present in ESR spectra (g = 2.004–2.005) [44].

In the electronic absorption spectra of $Fe(L^I)_2$, $Mn(L^I)_2$, $Fe(L^{II})_2$ and $Mn(H_2O)_2(L^{II})_2$ complexes in acetonitrile solution the absorption maxima in the high-energy region 225–305 nm belong to intraligand transitions (Sections 2.3.2, 2.3.3 and 2.3.5–2.3.6).

The absorption maxima appearing in the spectra of $Fe(L^I)_2$ and $Mn(L^I)_2$ at 310–315 and 410–490 nm are indicative of the ligand-to-metal(II) charge transfer transitions S → M^{II} and $O_{phenolate} \rightarrow M^{II}$, $O_{carboxylate} \rightarrow M^{II}$, respectively [45]. The spectra of the $Fe(L^{II})_2$ and $Mn(H_2O)_2(L^{II})_2$ complexes exhibit absorption bands at 315–345 nm which can be attributed to $O_{carboxylate} \rightarrow M^{II}$ and $O_{S=O} \rightarrow M^{II}$ charge transfer transitions [45,46].

According to the literature [45,47–49], the absorption maxima observed in the spectra of the complexes $Fe(L^I)_2$ (600 nm) and $Fe(L^{II})_2$ (560 nm) are due to *d*–*d* transitions characteristic of low-spin Fe(II) complexes with the octahedral and square planar geometry of FeS_2O_4 and FeO_4 coordination cores, respectively [48,50]. This conclusion is in agreement with ESR-spectroscopic data and values of effective magnetic moments for $Fe(L^I)_2$ and $Fe(L^{II})_2$ complexes, indicative of their diamagnetism (Sections 2.3.2 and 2.3.5). Hence, the field of the ligands HL^I and HL^{II} is strong enough for spin coupling in Fe(II) ion, and they form low-spin complexes with this ion. Spin coupling is also characteristic of Mn(II) ion in $Mn(L^I)_2$ and $Mn(H_2O)_2(L^{II})_2$ complexes, which is supported by the values of effective magnetic moment μ_{eff} of these complexes (Sections 2.3.3 and 2.3.6) [51]. Note that the absorption spectra of low-spin Mn(II) complexes with redox-active ligands have *d*–*d* bands at about 590–610 nm characteristic of the coordination octahedron [43,45,51–53]. These bands were found in the spectra of $Mn(L^I)_2$ and $Mn(H_2O)_2(L^{II})_2$ complexes, which may be indicative of the octahedral geometry of their MnS_2O_4 and MnO_6 chromophores (Sections 2.3.3 and 2.3.6).

The absorption maxima appearing in the spectra of $Fe(L^I)_2$, $Mn(L^I)_2$, $Fe(L^{II})_2$ and $Mn(H_2O)_2(L^{II})_2$ complexes at 640–665 nm are indicative of the metal(II)-to-ligand charge transfer transitions $M^{II} \rightarrow (\pi O)$ characteristic of low-spin complexes of redox-active ligands with readily oxidized ions of transition metals, specifically, Fe(II) and Mn(II) [45].

This view of coordination cores agrees with the data obtained by physico-chemical methods for other metal(II) complexes of the ligands HL^I and HL^{II} investigated previously [16]. The results obtained are verified by quantum chemical calculation of electronic and molecular structure of Cu(II), Ni(II), Zn(II), Fe(II) and Mn(II) complexes with these ligands. Co(II) complexes have not been included in calculations because of Co(II) complex with HL^I ligand being polymeric.

As quantum chemical calculations have auxiliary meaning with the respect to the aims of investigation, their results are presented in the discussion section in minimal necessary amount, but full results can be obtained from authors at request. As mentioned above, the coordination type can be specified by IR spectra analysis, while quantum chemical calculations provide a way of identifying *cis* or *trans* configuration of the metal complex. The comparison of the key low-frequency region in experimental and calculated for geometric isomers IR spectra, comprising the most specific vibrations of coordination core, was unambiguously indicative of *trans* configuration (Fig. 2).

In the light of the spectral data, magnetic moment values, analytical results and quantum chemical calculations the general mode of binding in the metal(II) complexes can be represented as shown below:

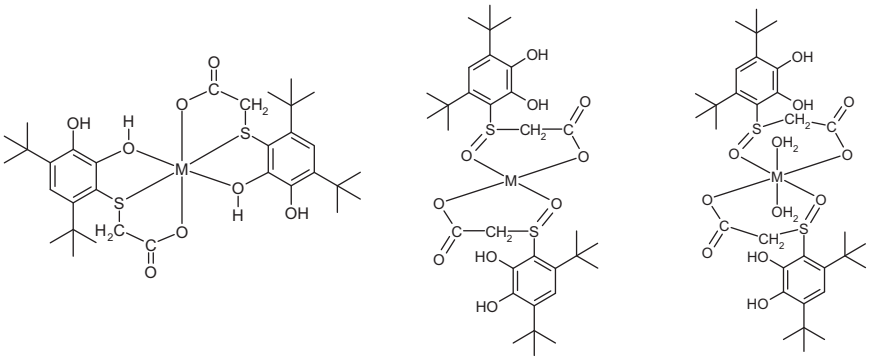

M=Cu(II), Ni(II), Fe(II), Mn(II) M=Cu(II), Co(II), Ni(II), Fe(II) M=Mn(II)

Cu(II), Ni(II) and Fe(II) complexes containing HL^{I} have the structure of A type (Fig. 1) (extremely distorted octahedron), while Mn(II) complex exists as B type structure, and the structure of the Zn(II) complex undergoes tetrahedral distortion. The general structure for complexes containing HL^{II} is of C type. Cu(II) and Fe(II) complexes are close to square planar ones, while those of Ni(II) and Zn(II) are nearly tetrahedral, and the coordination core of Mn(II) complex is octahedral (Table S1). When comparing respective geometry parameters of a free and a bound ligand (for example HL^{I} and $Ni(L^{I})_2$), one can see that noticeable changes occur only for the atoms involved in coordination and their neighbors (Table 1). Typical changes for the remote part of the ligand molecule do not exceed 1 pm of bond length and 2° of bond angle. For complexes of HL^{I} it is the inequality of phenolic oxygen atoms that attracts attention. The ^{I}O moves off from benzene ring, while ^{II}O approaches it during complexation.

To analyze the peculiarities of electronic structure of phenolic ligands and their complexes, the Mulliken population analysis has been performed. The rearrangement of electron density during complexation obviously must affect atomic charges; their evolution is given in Tables 2 and S2.

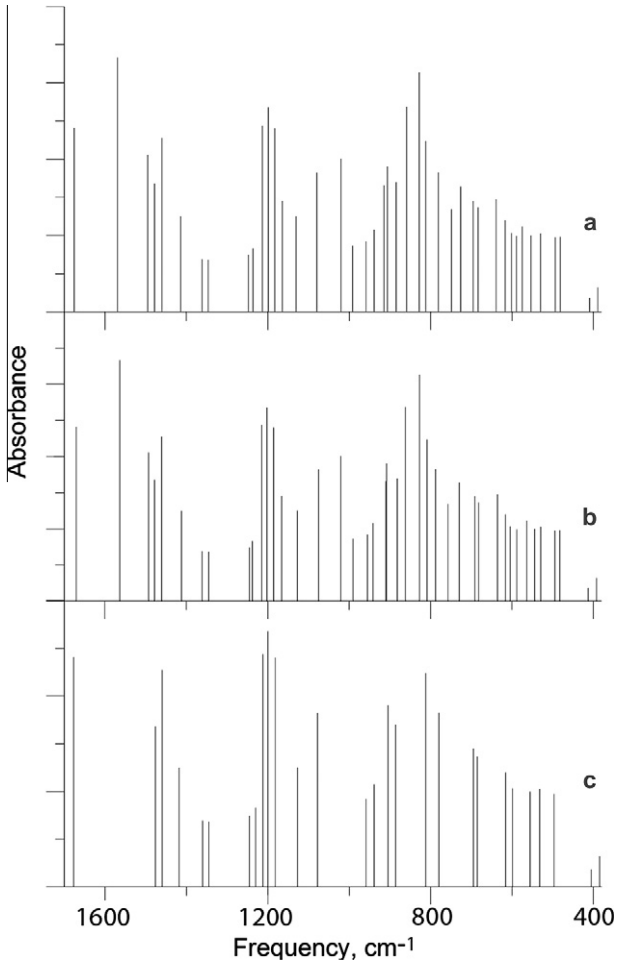

Fig. 2. Comparison of theoretical and experimental IR spectra of NiL^{I}_2 complex: (a) experimental, (b) *trans*, and (c) *cis*.

Table 1
Selected computed bond lengths (R, Å) and valence angles (α, °) for free ligands HL^{I}, HL^{II} and their complexes with Ni(II) ions.[a]

Parameter	HL^{I}	$Ni(L^{I})_2$	Parameter	HL^{II}	$Ni(L^{II})_2$
R(C–^{I}OH)	1.382	1.413	R(C–^{I}OH)	1.414	1.401
R(C–^{II}O)	1.378	1.360	R(C–^{II}OH)	1.381	1.357
R(C_{ar}–S)	1.780	1.784	R(C_{ar}–S)	1.836	1.828
R(C_{alk}–S)	1.827	1.863	R(C_{alk}–S)	1.871	1.822
α(C–S–C)	102.7	104.3	R(S–O)	1.514	1.561
α(S–C_{alk}–C_{carb})	113.0	104.6	α(C–S–C)	95.0	99.8

[a] Selected computed bond lengths (R, Å) and valence angles (α, °) for the complexes with Cu(II), Zn(II), Fe(II) and Mn(II) ions are given in Table S1.

Table 2
Selected computed Mulliken atomic charges (in electron charge units) for free ligands and their complexes with Ni(II) ions.[a]

Atom	HL^{I}	$Ni(L^{I})_2$	Atom	HL^{II}	$Ni(L^{II})_2$
Ni		0.271	Ni		0.534
^{II}O	−0.675	−0.593	^{II}O	−0.620	−0.659
S	0.252	0.319	S	0.974	0.949
C(–^{II}O)	0.287	0.357	C(–^{II}O)	0.327	0.337
C_{ar}(–S)	−0.289	−0.293	C_{ar}(–S)	−0.353	−0.340
C_{alk}(–S)	−0.698	−0.672	C_{alk}(–S)	−0.746	−0.670
H(–^{II}O)	0.410		H(–^{II}O)	0.396	0.461
C(=O, –OH)	0.681	0.649	C(=O, –OH)	0.640	0.642
^{III}O	−0.501	−0.442	^{V}O	−0.514	−0.664
^{IV}O	−0.549	−0.575	^{IV}O	−0.558	−0.530

[a] Selected computed atomic charges for the complexes with Cu(II), Zn(II), Fe(II) and Mn(II) ions are given in Table S2.

A noticeable change of charge occurs only for the atoms involved in coordination and adjacent atoms, which is rather logical. For phenolic oxygen atoms of HL^{I} it is only the deprotonated one that suffers charge increase, while for those of HL^{II} no major changes take place, suggesting another binding mode. The main contribution in metal electron density acquisition is provided by sulfur, deprotonated oxygen and adjacent carbon atoms for HL^{I} and remaining phenolic hydrogen atoms for both types of complexes.

Regarding the mechanism of donor–acceptor bond formation, the main input from ligand's HOMO and metal's LUMO can be expected. The frontier MO's of ligands and complexes are given in Fig. 3.

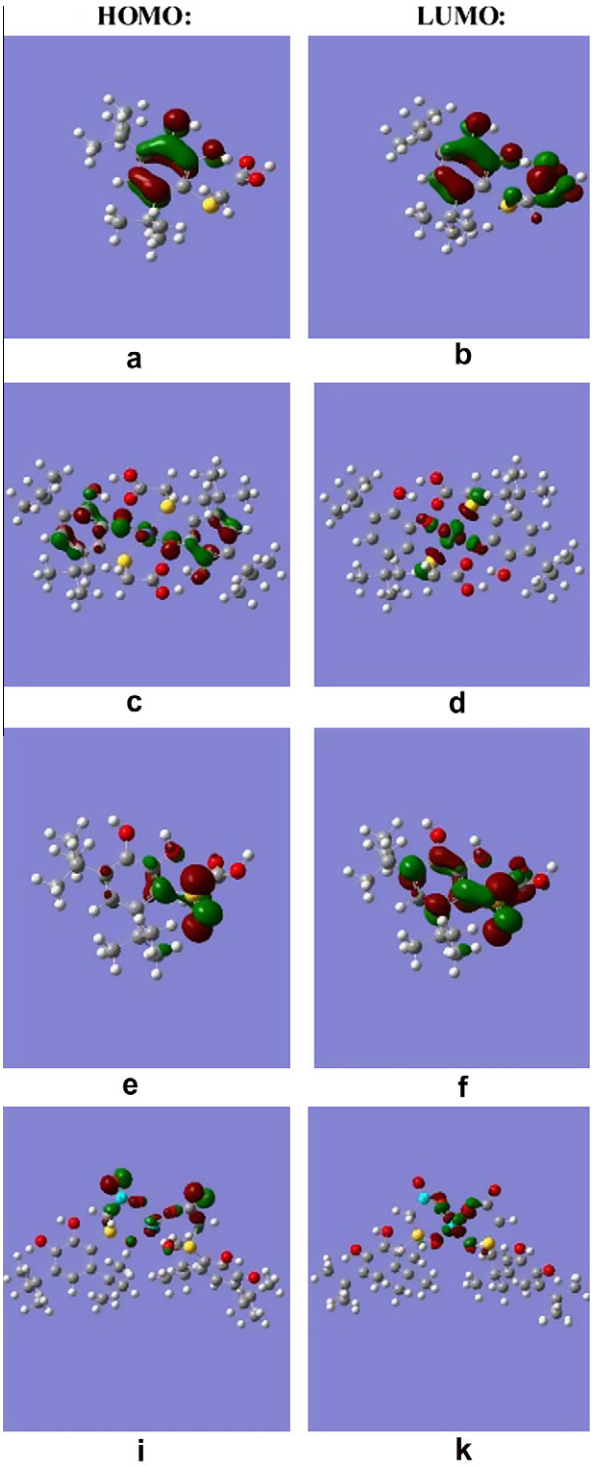

Fig. 3. The representation of frontier orbitals' surfaces for HL^{I} (a and b), HL^{II} (e and f) and their Ni(II) complexes (c, d, j, and k).

From the surfaces above one can see that for HL^{I} the main contribution into HOMO is made by oxygen and aromatic carbon atoms basis functions. It means that these positions are preferable for electrophilic attack, which is in agreement with HL^{I} coordination mode. For HL^{II} HOMO is localized mainly on sulfoxide group, whereas in its complexes the main input into HOMO is from directly bound oxygen atoms as well as carbonyl. Sulfur atoms basis functions make a negligible contribution into HOMO of both ligands and complexes, being presented in a deeper HOMO−1. The proximity of frontier orbitals of free ligands and metal complexes is responsible for their rather close redox properties.

3.2. Electrochemical studies

The data on redox properties of the compounds HL^{I} and HL^{II}, their metal complexes and 3,5-di(*tert*-butyl)pyrocatechin (HL^{III}) are presented in Table 3 and Fig. 4. It was taken into consideration that *o*-diphenol derivatives readily undergo electrochemical oxidation to give respective *o*-semiquinones and *o*-benzoquinones

Table 3
Cyclic voltammetry data (anodic scan) for the ligands HL^{I}, HL^{II} and their metal(II) complexes.

Compound	E_{pa} (V)	E_{pc} (V)	$E_{1/2}$ (V)	E_{pa} (V)	E_{pc} (V)	$E_{1/2}$ (V)	E_{pa} (V)	E_{pa} (V)
HL^{I}				1.26	0.64	0.95	1.54[a]	1.88[a]
$Cu(L^{I})_2$	0.41	0.14	0.28	1.20	0.57	0.88		1.76[a]
$Co(H_2O)_2L^{I}$								1.77[a]
$Ni(L^{I})_2$				1.39	0.64	1.02		1.76[a]
$Zn(L^{I})_2$				1.39	0.80	1.10		1.76[a]
$Fe(L^{I})_2$							1.55[a]	1.81[a]
$Mn(L^{I})_2$	0.79	0.30	0.55	1.22	0.48	0.85	1.54[a]	1.83[a]
HL^{II}				1.33	0.51	0.92		
$Cu(L^{II})_2$	0.68	0.18	0.43	1.33	0.69	1.01		
$Co(L^{II})_2$	0.94	0.17	0.55	1.33	0.68	1.01		
$Ni(L^{II})_2$	1.02	0.24	0.63	1.33	0.69	1.01		
$Zn(L^{II})_2$				1.81	0.50	1.16		
$Fe(L^{II})_2$	1.06	0.34	0.70					
$Mn(H_2O)_2(L^{II})_2$	0.80	0.50	0.65	1.30	0.65	0.90		
HL^{III}	1.20	0.45	0.83	1.40[a]				1.77[a]

[a] Irreversible process; it is just the anodic peak that is observed.

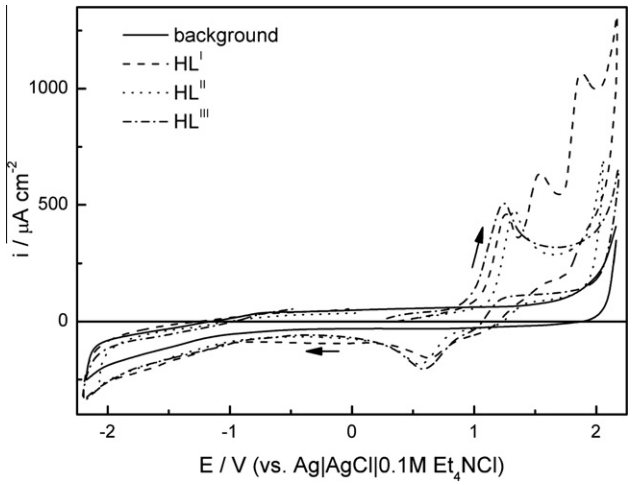

Fig. 4. Cyclic voltammograms (50 mV/s) of the ligands (1.36 mmol l^{-1}) HL^{I} (dashed line), HL^{II} (dotted line), HL^{III} (dashed–dotted line) in 0.1 mol l^{-1} $(C_2H_5)_4NClO_4$ acetonitrile solution on glassy-carbon electrode and background cyclic voltammogram of glassy-carbon electrode (solid line).

[54,55]; besides, oxidation of sulfur atom in the side chain of the ligands HL^{I} and HL^{II} is possible. The compound HL^{III}, lacking a sulfur-containing substituent, was used to carry out comparison studies of the redox conversions taking place.

On anodic potential scan *o*-diphenols HL^{I}, HL^{II} and HL^{III} undergo electrochemical oxidation reactions (Fig. 4). Comparing electrochemical data for these *o*-diphenols, one can note an anodic peak in the region 1.2–1.33 V, which is common for them, with a counterpart on the reverse scan, that is, a cathodic peak corresponding to reduction of oxidation products in the range of 0.45–0.64 V. Controlled electrolysis of solutions of these *o*-diphenols demonstrated that upon the anodic oxidation process associated with the peak at 1.20–1.33 V, the quantity of electricity passed corresponds to two electrons per molecule. In the absorption spectra of solutions containing products of their electrochemical oxidation there are bands at 400–470 nm which can be assigned to absorption of respective substituted *o*-benzoquinones [56]. Thus, it can be concluded that at the potentials of the first peak the *o*-diphenol derivatives HL^{I}, HL^{II} and HL^{III} undergo two successive one-electron oxidation processes to give *o*-benzoquinones, the cathodic peak corresponding to their reduction being observed in the range 0.45–0.64 V on the reverse scan. As this redox process for HL^{I}, HL^{II} and HL^{III} involves phenolic hydroxyls, the potentials of respective peaks are in a narrow range (Table 3), and it is only the compound HL^{II} that has a slightly different potential (1.33 V), which may be due to the acceptor effect of the sulfoxide group [57].

For the compounds HL^{II} and HL^{III} the above-mentioned peaks at the potentials E^{1}_{pa} and E^{1}_{pc} are the only ones, while for the compound HL^{I} there are several anodic peaks more (Fig. 4 and Table 3). Taking into account that the *o*-diphenol HL^{III} does not comprise sulfur-containing substituent, it may be suggested that in the case of *o*-diphenol derivative of thioglycolic acid HL^{I} it is successive oxidation processes involving sulfur atom and/or carboxylic group that take place at 1.54 and 1.88 V. Unlike HL^{I}, the compound HL^{II} has a sulfoxide lateral substitute, and a redox process involving sulfur atom of this group does not occur any more. This results in only one redox process involving hydroxyl groups of *o*-diphenol being observed for HL^{II} in the range under study (Fig. 4 and Table 3). No peaks corresponding to reduction of the compounds HL^{I}, HL^{II} and HL^{III} are observed upon cathodic polarization.

Characteristics of the redox processes observed in voltammograms of the metal complexes are presented in Table 3. The data obtained allow one to make conclusions about the reducing ability of the compounds under study. The investigation carried out showed that the ligand HL^{I} and its metal complexes can be arranged into a sequence according to their reducing ability, the formal potential of the redox system $E^{1}_{1/2}$ being used as its criterion (according to [58]): $Cu(L^{I})_2 > Mn(L^{I})_2 > HL^{I} > Ni(L^{I})_2 > Zn(L^{I})_2 > Fe(L^{I})_2 > Co(H_2O)_2L^{I}$. (The formal potential is calculated as the average potential of the peaks found by the cyclic voltammetry method: $E^{1}_{1/2} = (E^{1}_{pa} + E^{1}_{pc})/2$). On the basis of the electrochemical findings the ligand HL^{II} and its metal complexes can be graded in their reducing ability as follows: $Cu(L^{II})_2 > Co(L^{II})_2 > Ni(L^{II})_2 > Mn(H_2O)_2(L^{II})_2 > Fe(L^{II})_2 > HL^{II} > Zn(L^{II})_2$. The data on redox properties of the ligands and their metal complexes were used in interpreting the results of the biological evaluation of the compounds synthesized (Section 3.3).

3.3. Biological evaluation

3.3.1. Antibacterial activity

MIC values of the ligands HL^{I} and HL^{II} and their metal(II) complexes are listed in Table 4. It was for the first time that the antibacterial activity of Fe(II) and Mn(II) complexes of these ligands was investigated. For the ligands and their Cu(II), Co(II), Ni(II) and Zn(II) complexes, continuing our previous study [16], we have expanded the spectrum of Gram-positive – (*S. aureus*, *M. smegmatis*), Gram-negative bacteria (*S. typhimurium*) and carried out their microbiological investigation to compare the antibacterial activity of all the metal complexes under unified conditions (see Section 2.5).

Evaluating the antibacterial activity of the ligands and their metal(II) complexes, we can note that they demonstrated a low inhibiting ability toward Gram-negative bacteria: MIC >100 μg ml^{-1} (Table 4). Antibacterial activity of the ligands HL^{I} and HL^{II} and their metal(II) complexes against Gram-positive bacteria (*S. saprophiticus*, *S. aureus, B. subtilis, S. lutea*) is well higher than their activity against Gram-negative ones, and in some tests it is comparable to that of standard antibiotics (Table 4). The activity of the complexes $Cu(L^{I})_2$, $Mn(L^{I})_2$, $Cu(L^{II})_2$ and $Co(L^{II})_2$ against most of Gram-positive bacteria is higher than that of the ligands and other metal complexes under study; in particular, the high activity of these metal(II) complexes against *M. smegmatis* is worthy of particular notice. The pronounced change in activity resulting from complexation can be due to the growth in their lipophilicity (Table 5).

It has been found that the antibacterial activity of the metal(II) complexes synthesized does not correlate with the toxicity of the metal(II) ions to the bacteria tested, because none of the starting metal salts acts against bacteria up to the dose of 200 μg ml^{-1}. The antibacterial activity of the compounds examined follows

Table 4
Antibacterial activity of the free ligands and their metal(II) complexes evaluated by minimum inhibitory concentration (MIC, g ml^{-1}).

Compound	*Pseudomonas aeruginosa*	*Serratia marcescens*	*Salmonella typhimurium*	*Escherichia coli*	*Bacillus subtilis*	*Sarcina lutea*	*Staphylococcus saprophyticus*	*Staphylococcus aureus*	*Mycobacterium smegmatis*
HL^{I}	>100	>100	>100	>100	50	25	25	25	12.5
$Cu(L^{I})_2$	>100	>100	>100	>100	25	12.5	6.2	6.2	6.2
$Co(H_2O)_2L^{I}$	>100	>100	>100	>100	>100	100	50	50	100
$Ni(L^{I})_2$	>100	>100	>100	>100	>100	50	25	25	25
$Zn(L^{I})_2$	>100	>100	>100	>100	>100	50	25	25	100
$Fe(L^{I})_2$	>100	>100	>100	>100	100	50	50	100	50
$Mn(L^{I})_2$	>100	>100	>100	>100	50	12.5	25	12.5	6.2
HL^{II}	>100	>100	>100	>100	>100	50	100	50	50
$Cu(L^{II})_2$	>100	>100	>100	>100	25	12.5	12.5	6.2	6.2
$Co(L^{II})_2$	>100	>100	>100	>100	25	12.5	25	12.5	6.2
$Ni(L^{II})_2$	>100	>100	>100	>100	25	12.5	50	25	25
$Zn(L^{II})_2$	>100	>100	>100	>100	>100	100	50	50	100
$Fe(L^{II})_2$	>100	>100	>100	>100	>100	25	50	50	25
$Mn(H_2O)_2(L^{II})_2$	>100	>100	>100	>100	50	12.5	50	50	25
Streptomycin	>100	6.2	12.5	3.1	6.2	12.5	6.2	6.2	3.1
Tetracycline			6.2	3.1	6.2	6.2	6.2	3.1	
Chloramphenicol	12.5		6.2	6.2	3.1		6.2	6.2	12.5

Table 5
Octanol/water partition coefficients ($\log P_{ow}$) of the ligands and metal complexes.[a]

Compound	$\log P_{ow}$
$Fe(L^I)_2$	5.26
$Mn(L^I)_2$	3.06
$Fe(L^{II})_2$	5.39
$Mn(H_2O)_2(L^{II})_2$	3.08

[a] $\log P_{ow}(HL^I) = 2.31$; $\log P_{ow}(HL^{II}) = -2.07$; $\log P_{ow}$ of the Cu(II), Co(II), Ni(II) and Zn(II) complexes with the ligands HL^I and HL^{II} varies in the range 3–5 [16].

the order: (1) $Cu(L^I)_2 > Mn(L^I)_2 > HL^I > Ni(L^I)_2 > Zn(L^I)_2 > Fe(L^I)_2 > Co(H_2O)_2L^I$; (2) $Cu(L^{II})_2 > Co(L^{II})_2 > Ni(L^{II})_2 > Mn(H_2O)_2(L^{II})_2 > Fe(L^{II})_2 > HL^{II} > Zn(L^{II})_2$; their reducing ability (determined electrochemically) follows the same order, as it was shown above (Table 3).

Thus, $Cu(L^I)_2$, $Mn(L^I)_2$, $Cu(L^{II})_2$ and $Co(L^{II})_2$ complexes characterized by a strong antibacterial activity demonstrate a much higher reducing ability than that of the ligands and the rest of the metal complexes. These complexes may be considered as potential antimicrobial agents, particularly when their activity is comparable with the inhibiting effect of streptomycin, tetracycline and chloramphenicol (Table 4).

Table 6
Rates of reduction of Cyt *c* (v) with the ligands HL^I, HL^{II}, and their metal(II) complexes.[a]

Compound	v (nmol min^{-1})
HL^I	1.0
$Cu(L^I)_2$	6.1
$Co(H_2O)_2L^I$	2.1
$Ni(L^I)_2$	0.5
$Zn(L^I)_2$	0.8
$Fe(L^I)_2$	0.5
$Mn(L^I)_2$	4.4
HL^{II}	1.1
$Cu(L^{II})_2$	3.1
$Co(L^{II})_2$	5.4
$Ni(L^{II})_2$	3.0
$Zn(L^{II})_2$	3.5
$Fe(L^{II})_2$	2.2
$Mn(H_2O)_2(L^{II})_2$	2.3

[a] The final concentrations of Cyt *c* and the complex (or the ligand) were respectively 7 and 35 μmol l^{-1}.

3.3.2. Reduction of cytochrome c

The results of spectrophotometric investigation of redox interaction of oxidized form of Cyt *c* with the HL^I and HL^{II} ligands and their Cu(II), Co(II), Ni(II), Zn(II), Mn(II) and Fe(II) complexes are given in Table 6. The characteristic absorption bands at 550 and 520 nm appearing when the ligands or their metal complexes are added to the solution of the oxidized Cyt *c* bear witness to the ability of these compounds to reduce Cyt *c in vitro* [59,60].

We have found that the rate of Cyt *c* reduction with HL^{II} ligand corresponds to that with HL^I ligand (Table 3). Taking into account the findings presented in [59–61], it can be suggested that the most probable route of oxidation of the ligands HL^I and HL^{II} in the system of interest *in vitro* under anaerobic conditions involves single-electron stages of their anionic or molecular forms being oxidized to *o*-benzoquinones upon interacting with Cyt *c* via intermediate formation of respective *o*-benzosemiquinone (Fig. 5).

Almost equal rates of Cyt *c* reduction with HL^I and HL^{II} ligands can be due first of all to similar reducing abilities of these compounds (Table 3). Furthermore, their ionization constants, characterizing their ability to form anions by hydroxyls being deprotonated, differ but slightly ($pK(HL^I) = 8.3$ and $pK(HL^{II}) = 7.9$ [16]).

In the series of metal complexes with HL^I ligand it is $Cu(L^I)_2$ and $Mn(L^I)_2$ complexes that show the highest rate of Cyt *c* reduction, higher than the rate of redox process involving the free ligand (Table 6). It should be emphasized that, according to electrochemical data, these complexes are the most active reducing agents in the series of metal complexes with the ligand HL^I (Table 3). $Co(H_2O)_2L^I$ complex can reduce Cyt *c in vitro* in the system under study faster than Ni(II), Zn(II), Fe(II) complexes and HL^I ligand do (Table 6), although it has the lowest reducing ability among the complexes of this series (Table 3). It should be taken into account that metal complexes can interact with Cyt *c* both in their molecular form and via phenolate ligand and metal ions formed upon their dissociation [60]. In this connection attention should be paid to the values of stability constant of these metal complexes: $Cu(L^I)_2$ ($\log\beta = 7.1$) and $Cu(L^{II})_2$ ($\log\beta = 7.3$) are the most stable ones among the metal complexes, while $Co(H_2O)_2L^I$ is the most ready to dissociate ($\log\beta = 3.5$) [16].

All the metal complexes with the ligand HL^{II} reduce Cyt *c* at a rate several times higher than that of the redox process involving the free ligand (Table 6). It is $Co(L^{II})_2$ complex that is characterized

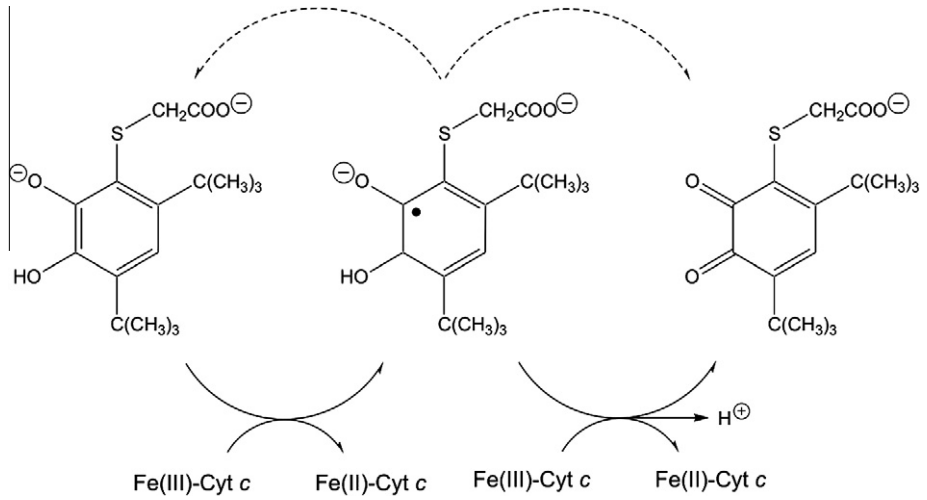

Fig. 5. Scheme of the reduction of Cyt *c* with the anion form of the ligand HL^I; Fe(III)–Cyt *c* and Fe(II)–Cyt *c* – respectively the oxidized and reduced forms of Cyt *c*; the process of disproportionation of the ligand HL^I is depicted by a dashed line.

Table 7
Effect of electron-transfer proteins of P450-dependent monooxygenase systems on the rate of Cyt *c* (7 μmol l^{-1}) reduction (*v*) with HL^{I} and HL^{II} ligands (35 μmol l^{-1}).

Ligand	Enzyme/concentration (nmol l^{-1})	*v* (nmol min^{-1})
HL^{I}		0.9 ± 0.1
HL^{I}	P450R/170	0.8 ± 0.1
HL^{I}	P450R/270	0.9 ± 0.1
HL^{II}		1.0 ± 0.1
HL^{II}	P450R/170	0.9 ± 0.1
HL^{II}	P450R/270	0.9 ± 0.1

Table 8
Calculated parameters for docked conformations of the ligands to P450R.

Ligand	Lateral groups	L_{min}(O–N) (Å)/K_{int} (mmol l^{-1})	K_{int} range (mmol l^{-1})
HL^{I}	$-CO_2H$	3.1/86.9	17.7–147.6
HL^{II}	$-CO_2H$	6.4/63.3	14.1–152.3
HL^{IV}	$-CH_2OH$	3.5/1.4	1.4–14.2
HL^{V}	$-CH_3$	2.9/5.2	2.6–7.1

by the highest Cyt *c* reduction rate, thus being one of the strongest reducing agents in this series of complexes. $Cu(L^{II})_2$ complex, in spite of the most cathodic $(E^{a}_{p1} + E^{c}_{p1})/2$ value among these compounds, ranks below $Co(L^{II})_2$ complex in the rate of Cyt *c* reduction (Table 6), which may be due to its being more stable to dissociation as compared to the above-mentioned complexes. The rate of Cyt *c* reduction with the rest of the metal complexes with the ligand HL^{II} varies in a very narrow range (2–3 nmol min^{-1}) and does not correlate with their reducing ability determined electrochemically (Tables 3 and 6).

The influence of P450R on the rate of Cyt *c* reduction with HL^{I} and HL^{II} ligands was studied. The addition of P450R had essentially no effect on the initial rate of Cyt *c* reduction with the compounds under study (Table 7), as opposed to the phenolic ligands 4,6-di(-*tert*-butyl)-3[(2-ethyl)sulfanyl]-1,2-dihydroxybenzene (HL^{IV}) and 2-amino-4,6-di(*tert*-butyl)phenol studied before [7]. This is indicative of *o*-diphenol derivatives of thioglycolic acid being incapable of redox interactions with P450R, responsible for an increase of Cyt *c* reduction *in vitro* in the system described. In this connection we have studied Cyt *c* reduction and P450R affecting this process with the participation of a structural analog of *o*-diphenol derivatives of thioglycolic acid, 4,6-di(*tert*-butyl)-3-ethylsulfanyl-1,2-dihydroxybenzene (HL^{V}), containing a lateral methyl group instead of a carboxylic one. The rate of Cyt *c* reduction with this compound was found to be 0.7 ± 0.1 nmol Cyt $c \times min^{-1}$, and it is about twice as high as that with P450R added. Analyzing structure-functional differences of these ligands, we can reveal probable reasons for this effect: (i) a smaller reductive ability of the ligands HL^{I} and HL^{II} compared to the *o*-diphenol and *o*-aminophenol derivatives studied before [7], (ii) lateral carboxylic groups of HL^{I} and HL^{II} ligands being negatively charged at physiological pH 7.4.

It should be mentioned that redox-active FMN edge in P450R is surrounded by several negatively charged residues of Glu and Asp amino acids located on the protein surface. To evaluate the supposed contribution of electrostatic repulsion into P450R interaction with the ligands under study, we carried out docking experiments of the above-mentioned ligand structures in the active center of P450R according to the procedure described in [33–35]. Millimolar order of K_{int} values calculated from the docking results suggests the non-specific character of P450R interaction with all the compounds described above, but the compounds HL^{IV} and HL^{V} were more effectively bound in the vicinity of FMN than *o*-diphenol derivatives of thioglycolic acid HL^{I} and HL^{II} under *in silico* conditions (Table 8).

4. Conclusions

The complexes $Cu(L^{I})_2$, $Mn(L^{I})_2$ and $Co(L^{II})_2$ with the high reducing ability (determined electrochemically) were found to be characterized by the highest rates of Cyt *c* reduction. As a whole, the reduction of Cyt *c* by the ligands and their metal complexes may not be related solely to the facility of their oxidation, as it is possible that ionization of the compounds exerts a noticeable effect on this process, too. The antibacterial activity of these compounds was found to follow the order: (1) $Cu(L^{I})_2 > Mn(L^{I})_2 > HL^{I} > Ni(L^{I})_2 > Zn(L^{I})_2 > Fe(L^{I})_2 > Co(H_2O)_2L^{I}$; (2) $Cu(L^{II})_2 > Co(L^{II})_2 > Ni(L^{II})_2 > Mn(H_2O)_2(L^{II})_2 > Fe(L^{II})_2 > HL^{II} > Zn(L^{II})_2$; their reducing ability (determined electrochemically) followed the same order. These sequences are not entirely the same as those characterizing the decrease of the rates of Cyt *c* reduction with the ligands and their metal complexes. Despite the fact that in individual cases we have found a correlation between the rates of Cyt *c* reduction and physico-chemical characteristics of the compounds under study, the ability of bioactive compounds to interact with biomolecules has a more intricate dependence on the structure and physico-chemical properties thereof.

Appendix A. Supplementary data

Supplementary data associated with this article can be found, in the online version, at doi:10.1016/j.poly.2011.07.008.

References

[1] N.V. Loginova, T.V. Koval'chuk, R.A. Zheldakova, A.A. Chernyavskaya, N.P. Osipovich, G.K. Glushonok, G.I. Polozov, V.L. Sorokin, O.I. Shadyro, Centr. Eur. J. Chem. 4 (2006) 440.
[2] T.V. Koval'chuk, N.V. Loginova, G.I. Polozov, A.A. Chernyavskaya, D.A. Gursky, O.I. Shadyro, Vestnik BGU. Ser. 2. Khim., Biol. Geogr. (2) (2008) 25 (in Russian).
[3] N.V. Loginova, T.V. Koval'chuk, R.A. Zheldakova, A.A. Chernyavskaya, N.P. Osipovich, G.K. Glushonok, G.I. Polozov, V.N. Povalishev, V.L. Sorokin, O.I. Shadyro, Polyhedron 25 (2006) 3603.
[4] N.V. Loginova, T.V. Koval'chuk, R.A. Zheldakova, N.P. Osipovich, V.L. Sorokin, G.I. Polozov, G.A. Ksendzova, G.K. Glushonok, A.A. Chernyavskaya, O.I. Shadyro, Bioorg. Med. Chem. Lett. 16 (2006) 5403.
[5] N.V. Loginova, T.V. Koval'chuk, N.P. Osipovich, G.I. Polozov, V.L. Sorokin, A.A. Chernyavskaya, O.I. Shadyro, Polyhedron 27 (2008) 985.
[6] N.V. Loginova, T.V. Koval'chuk, G.I. Polozov, N.P. Osipovich, P.G. Rytik, I.I. Kucherov, A.A. Chernyavskaya, V.L. Sorokin, O.I. Shadyro, Eur. J. Med. Chem. 43 (2008) 1536.
[7] N.V. Loginova, Y.V. Faletrov, T.V. Koval'chuk, N.P. Osipovich, G.I. Polozov, A.A. Chernyavskaya, R.A. Zheldakova, I.I. Azarko, A.T. Gres', O.I. Shadyro, V.M. Shkumatov, Polyhedron 29 (2010) 1646.
[8] A. Albert, Selective Toxicity: Physico-Chemical Basis of Therapy, Chapman and Hall, London, New York, 1985.
[9] S. Bollo, L.J. Núñez-Vergara, S. Kang, L. Zhang, H.I. Boshoff, C.E. Barry III, J.A. Squella, C.S. Dowd, Bioorg. Med. Chem. Lett. 21 (2011) 812.
[10] B. Wen, K.J. Coe, P. Rademacher, W.L. Fitch, M. Monshouwer, S.D. Nelson, Chem. Res. Toxicol. 21 (2008) 2393.
[11] J. Simon, FEMS Microbiol. Rev. 26 (2002) 285.
[12] J. Hendriks, A. Oubrie, J. Castresana, A. Urbani, S. Gemeinhardt, M. Saraste, Biochim. Biophys. Acta 1459 (2000) 266.
[13] L. De Smet, S.N. Savvides, E. Van Horen, G. Pettigrew, J.J. Van Beeumen, J. Biol. Chem. 281 (2006) 4371.
[14] I. Bertini, G. Cavallaro, A. Rosato, Chem. Rev. 106 (2006) 90.
[15] L. Thony-Meyer, Microbiol. Mol. Biol. Rev. 61 (1997) 337.
[16] N.V. Loginova, T.V. Koval'chuk, G.I. Polozov, N.P. Osipovich, A.A. Chernyavskaya, V.L. Sorokin, O.I. Shadyro, Redox-active antimicrobial metal complexes with sterically hindered *o*-diphenol and *o*-aminophenol derivatives, in: G. Blanc, D. Moreau (Eds.), Biometals: Molecular Structures, Binding Properties, Nova Science Publisher's, Hauppauge, New York, 2010, pp. 59–90.
[17] M. Buhl, H. Kabrede, J. Chem. Theory Comput. 2 (2006) 1282.
[18] T. Wang, G. Brudvig, V.S. Batista, J. Chem. Theory Comput. 6 (2010) 755.
[19] Y. Yang, M.N. Weaver, K.M. Merz, J. Phys. Chem. A 113 (2009) 9843.
[20] Z. An, J. Zhang, R. Wang, N. Koga, Polyhedron 26 (2007) 2126.
[21] K. Malek, H. Kozlowski, L.M. Proniewicz, Polyhedron 24 (2005) 1175.
[22] A. Leo, C. Hansch, D. Elkins, Chem. Rev. 71 (1971) 525.
[23] M.J. Frisch, G.W. Trucks, H.B. Schlegel, G.E. Scuseria, M.A. Robb, J.R. Cheeseman, J.A. Montgomery Jr., T. Vreven, K.N. Kudin, J.C. Burant, J.M. Millam, S.S. Iyengar, J. Tomasi, V. Barone, B. Mennucci, M. Cossi, G. Scalmani, N. Rega, G.A. Petersson, H. Nakatsuji, M. Hada, M. Ehara, K. Toyota, R. Fukuda, J. Hasegawa,

M. Ishida, T. Nakajima, Y. Honda, O. Kitao, H. Nakai, M. Klene, X. Li, J.E. Knox, H.P. Hratchian, J.B. Cross, C. Adamo, J. Jaramillo, R. Gomperts, R.E. Stratmann, O. Yazyev, A.J. Austin, R. Cammi, C. Pomelli, J.W. Ochterski, P.Y. Ayala, K. Morokuma, G.A. Voth, P. Salvador, J.J. Dannenberg, V.G. Zakrzewski, S. Dapprich, A.D. Daniels, M.C. Strain, O. Farkas, D.K. Malick, A.D. Rabuck, K. Raghavachari, J.B. Foresman, J.V. Ortiz, Q. Cui, A.G. Baboul, S. Clifford, J. Cioslowski, B.B. Stefanov, G. Liu, A. Liashenko, P. Piskorz, I. Komaromi, R.L. Martin, D.J. Fox, T. Keith, M.A. Al-Laham, C.Y. Peng, A. Nanayakkara, M. Challacombe, P.M.W. Gill, B. Johnson, W. Chen, M.W. Wong, C. Gonzalez, J.A. Pople, GAUSSIAN 03, Revision C, Gaussian Inc., Pittsburgh, PA, 2003.

[24] P.J. Hay, W.R. Wadt, J. Chem. Phys. 82 (1985) 299.

[25] J.W. Ponder, Tinker Software, Version 5.0, 2010, http://dasher.wustl.edu/tinker.

[26] D.C. Young, Computational Chemistry: A Practical Guide for Applying Techniques to Real-World Problems, Wiley Interscience, New York, 2001.

[27] A.V. Aleshukina, Medicinal Microbiology, Phoenix, Rostov-on-Don, 2003 (in Russian).

[28] A.A. Akhrem, N.V. Lapko, A.G. Lapko, V.M. Shkumatov, V.L. Chashchin, Acta Biol. Med. Ger. 38 (1979) 257.

[29] S. Tamura, K.R. Korzekwa, S. Kimura, H.V. Gelboin, F.J. Gonzalez, Arch. Biochem. Biophys. 293 (1992) 219.

[30] C.C. Winterbourn, Biochem. J. 207 (1982) 609.

[31] G.F.Z. da Silva, W.M. Tay, Li-J. Ming, J. Biol. Chem. 280 (2005) 16601.

[32] N. Rahman, Y. Ahmad, S.N.H. Azmi, AAPS PharmSciTech. 6 (2005) 543.

[33] G.M. Morris, D.S. Goodsell, R.S. Halliday, R. Huey, W.E. Hart, R.K. Belew, A.J. Olson, J. Comput. Chem. 19 (1998) 1639.

[34] M.F. Sanner, J. Mol. Graphics Mod. 17 (1999) 57.

[35] J. Gasteiger, M. Marsili, Tetrahedron 36 (1980) 3219.

[36] W.J. Geary, Coord. Chem. Rev. 7 (1971) 81.

[37] C.N. Verani, Rational Synthesis and Characterization of Paramagnetic Heteropolynuclear Systems, Ph.D. Thesis, Ruhr-Universität Bochum, Mülheim an der Ruhr, 2000.

[38] C.J. Cramer, D.G. Truhlar, Phys. Chem. Chem. Phys. 11 (2009) 10757.

[39] W. Koch, M.C. Holthausen, A Chemist's Guide to Density Functional Theory, Wiley-VCH, 2000.

[40] K. Nakamoto, Infrared and Raman Spectra of Inorganic and Coordination Compounds: Theory and Applications in Inorganic Chemistry, John Wiley and Sons Inc., New York, 1997.

[41] L.J. Bellamy, The Infrared Spectra of Complex Molecules, Methuen, London, 1958.

[42] S. Belaid, S. Djebbar, O. Benali-Baitich, M. Khan, G. Bouet, J. Inorg. Biochem. 102 (2008) 63.

[43] A. Carrington, E. MacLachlan, Introduction to Magnetic Resonance with Applications to Chemistry and Chemical Physics, Harper and Row, New York, 1967.

[44] A.D. Shultz, A.K. Boal, D.J. Driscoll, J.R. Kitchin, G.N. Tew, J. Org. Chem. 60 (1995) 3578.

[45] A.B.P. Lever, E.I. Solomon (Eds.), Inorganic Electronic Structure and Spectroscopy, John Wiley and Sons, New York, 2006.

[46] A. Pui, J.-P. Mahy, Polyhedron 26 (2007) 3143.

[47] A.M. Shaker, M.Sh. Adam, Synth. React. Inorg. Met.-Org. Chem. 33 (2003) 1081.

[48] M.J. Sever, J.J. Wilker, J. Chem. Soc., Dalton Trans. (2004) 1061.

[49] M.L. Childers, J. Cho, C.A.S. Regino, M.W. Brechbiel, A.G. DiPasquale, A.L. Rheingold, S.V. Torti, F.M. Torti, R.P. Planalp, J. Inorg. Biochem. 102 (2008) 150.

[50] N.R. Perron, J.N. Hodges, M. Jenkins, J.L. Brumaghim, Inorg. Chem. 47 (2008) 6153.

[51] A. Saha, P. Majumdar, S. Goswami, J. Chem. Soc., Dalton Trans. (2000) 1703.

[52] M.J. Sabater, A. Corma, J.V. Folgado, H. García, J. Phys. Org. Chem. 13 (2000) 57.

[53] J.J. Alexander, H.B. Gray, J. Am. Chem. Soc. 90 (1968) 4260.

[54] G. Speier, Z. Tyeklar, P. Toth, E. Speier, S. Tisza, A. Rochen-bauer, A.M. Whalen, N. Alkire, C.G. Pierpont, Inorg. Chem. 40 (2001) 5653.

[55] C.G. Pierpont, Coord. Chem. Rev. 216–217 (2001) 99.

[56] F. Zippel, F. Ahlers, R. Werner, W. Haase, H.F. Nolting, B. Krebs, Inorg. Chem. 35 (1996) 3409.

[57] N.T. Berberova, I.V. Smolyaninov, A.O. Okhlobystin, N.N. Letichevskaya, E.V. Shinkar, Mend. Chem. J. 59 (5) (2005) 67 (in Russian).

[58] F. Scholz, Electroanalytical Methods: Guide to Experiments and Applications, Springer-Verlag, Berlin, 2002.

[59] H.T. Nagasawa, H.R. Gutmann, M.A. Morgan, J. Biol. Chem. 234 (1958) 1600.

[60] M.M.M. Saleem, M.T. Wilson, Biochem. J. 201 (1982) 433.

[61] E.L. Cavalieri, K.M. Li, N. Balu, M. Saeed, P. Devanesan, S. Higginbotham, J. Zhao, M.L. Gross, E.G. Rogan, Carcinogenesis 6 (2002) 1071.